

Beyond the Largest Lyapunov Exponent: Entropy-Based Diagnostics of Chaos in Hénon-Heiles and N -Body Dynamics

Alessandro Alberto Trani^{1,2}, Pierfrancesco Di Cintio^{3,4,5}, and Michele Ginolfi^{3,6}

¹ Department of Astronomy, University of Concepción, Avenida Esteban Iturra s/n Casilla 160-C Concepción, Chile

² National Institute for Nuclear Physics – INFN, Sezione di Trieste, I-34127, Trieste, Italy
e-mail: aatrani@gmail.com

³ National Institute of Astrophysics - Arcetri Astrophysical Observatory (INAF-OAA), Piazzale E. Fermi 5, I-50125 Firenze, Italy

⁴ National Council of Research - Institute of Complex Systems, Via Madonna del piano 10, I-50019 Sesto Fiorentino, Italy

⁵ National Institute of Nuclear Physics (INFN) - Florence unit, via G. Sansone 1, I-50019 Sesto Fiorentino, Italy
e-mail: pierfrancesco.dicintio@cnr.it

⁶ University of Florence, Department of Physics and Astronomy - Astrophysics and Space Science section, Piazzale E. Fermi 5, I-50125 Firenze, Italy
e-mail: michele.ginolfi@unifi.it

Received M DD, YYYY; accepted M DD, YYYY

ABSTRACT

Context. The largest Lyapunov exponent is widely used to diagnose chaos in gravitational dynamics, but in mixed phase spaces and finite- N systems it does not always provide a complete description of orbital complexity and phase-space transport. Entropy-based diagnostics may offer a complementary perspective.

Aims. We investigate whether trajectory-based information entropy can provide a useful diagnostic of chaos in gravitational systems and how it relates to the largest Lyapunov exponent as a function of orbital energy and of the number of degrees of freedom.

Methods. We computed the largest Lyapunov exponent and a coarse-grained Shannon entropy for ensembles of trajectories in the Hénon-Heiles potential and for test-particle orbits in live N -body realizations of a Plummer model. We then compared the dependence of both quantities on orbital energy and, for the N -body case, on particle number.

Results. In the Hénon-Heiles system, the Shannon entropy follows the transition from weak to widespread chaos and exhibits an energy dependence that closely mirrors that of the largest Lyapunov exponent. For test-particle orbits in live N -body potentials, both diagnostics indicate stronger chaos for more tightly bound trajectories. However, their dependence on N differs: the largest Lyapunov exponent remains nearly constant over the explored range of particle numbers, whereas the Shannon entropy decreases monotonically as N increases.

Conclusions. These results show that the Shannon information entropy can complement the largest Lyapunov exponent and may better capture changes in global phase-space mixing, especially in systems where the leading Lyapunov exponent alone is not sufficiently informative. It therefore provides a promising alternative for diagnosing chaos when tangent-space dynamics is unavailable, prohibitively expensive, or slowly convergent. In particular, because this entropy measure relies only on time series of phase-space coordinates, it is naturally suited to systems with densely sampled trajectories, such as minor bodies in the Solar System.

Key words. Chaos – Celestial mechanics – Methods: numerical – Diffusion

1. Introduction

Gravitational systems, even for relatively low numbers of degree of freedom, are known to be characterized by the coexistence of regular and chaotic orbits, the latter typically dubbed in a loose sense as “having a strong dependence on their initial conditions” (Contopoulos 2002). The main open issues surrounding chaos in the gravitational N -body problem can be summarized as follows: (1) the relation between Hamiltonian chaos and the onset and dynamical instabilities in the few body systems (Milani & Nobili 1992; Batygin & Laughlin 2008; Mogavero et al. 2023); (2) the dependence of the degree of chaos on the specific orbital structure of a given energy landscape in galactic potentials (Carpintero & Aguilar 1998; Karanis & Caranicolas 2001; Kandrup & Siopis 2003); (3) the scaling of such degree of chaos with the number of degrees of freedom of the systems at hand (Miller 1971; Gurzadyan & Savvidy 1986; Kandrup & Smith 1991; Goodman et al. 1993; Kandrup & Sideris 2001; El-Zant

et al. 2019; Di Cintio & Casetti 2019; Portegies Zwart et al. 2023).

Usually, the degree of chaos in an autonomous dynamical system that can be expressed in Hamiltonian form $\mathcal{H}(x_1, p_1, \dots, x_N, p_N) = \text{const}$ is estimated by evaluating numerically its largest Lyapunov exponent (e.g. see Lichtenberg & Leiberman 1992), formally defined by

$$\lambda_{\max} = \lim_{t \rightarrow \infty} \lim_{\|\mathbf{W}_0\| \rightarrow 0} \frac{1}{t} \ln \frac{\|\mathbf{W}(t)\|}{\|\mathbf{W}_0\|} . \quad (1)$$

In the equation above, $\mathbf{W} = (\delta x_1, \delta p_1, \dots, \delta x_N, \delta p_N)$ denotes the state vector in the tangent space \mathcal{S}_T to the phase space \mathcal{S} of the system. The dynamics of the tangent vectors is given by

$$\delta \dot{\mathbf{x}} = \delta \mathbf{p}; \quad \delta \dot{\mathbf{p}} = -\mathbf{D}_V^2(\mathbf{x}) \delta \mathbf{x}, \quad (2)$$

where $\mathbf{x} = (x_1, \dots, x_N)$, and analogously for $\delta \mathbf{x}$, \mathbf{p} and $\delta \mathbf{p}$ and

$$\mathbf{D}_V^2(\mathbf{x})_{jk} = \left. \frac{\partial^2 V(\mathbf{x})}{\partial x_j \partial x_k} \right|_{\mathbf{x}}; \quad j, k = 1, 2, \dots, N, \quad (3)$$

where $V(\mathbf{x})$ is the potential part of the Hamiltonian $\mathcal{H} = \mathbf{p}^2/2 + V(\mathbf{x})$.

If computing the matrix D_V^2 is particularly cumbersome, or if the system is non-autonomous (i.e. \mathcal{H} has an explicit dependence on time), one typically replaces the norm of the tangent vector $\|\mathbf{W}(t)\|$ in Eq. (1) with the phase-space distance between two initially nearby trajectories $\xi(t)$ and $\xi'(t)$ (Benettin et al. 1980). In this case, the numerically estimated λ_{\max} may depend on the initial normalization of \mathbf{W}_0 , unless periodic renormalization is applied.

More generally, the full Lyapunov spectrum can be computed by propagating the variational equations up to a time τ , after which the tangent vectors are orthonormalized (e.g. via a Gram–Schmidt procedure) to prevent their alignment with the most unstable direction (Wiesel 1993; Christiansen & Rugh 1997; Quarles et al. 2011). The finite-time Lyapunov exponents $\lambda_i(\tau)$ are then obtained by accumulating the logarithmic growth factors associated with the orthonormalization:

$$\lambda_i(\tau) = \frac{1}{\tau} \left(\lambda_{i-1}(\tau) + \ln \left\| \mathbf{z}_i - \sum_{j=1}^i \langle \mathbf{z}_i, \mathbf{z}'_{j-1} \rangle \mathbf{z}'_{j-1} \right\| \right), \quad (4)$$

up to the desired precision dictated by the chosen convergence criterion. In Eq. (4), $\mathbf{z}_i = (\delta x_i, \delta p_i)$ denotes the i -th deviation (tangent) vector, initially normalized to unity, and $\lambda_0 = 0$.

Using the Lyapunov exponent as a metric of chaos to investigate its scaling in the continuum limit of the N -body problem (i.e. $N \rightarrow \infty$ with asymptotically vanishing individual particle mass), leads to puzzling findings. For a given model, determined by a potential density pair supported by an equilibrium phase-space distribution f , single particle trajectories, reasonably independently of their specific energies, resemble more and more their parent realizations in the smooth potential of the continuum model, while their maximal Lyapunov exponents depend weakly on the number of simulation particles N .

Kandrup & Sideris (2001) using frozen N -body experiments (i.e. test particles propagated through the potential generated by a distribution of N fixed particles sampling a given density profile), concluded that chaos associated with discreteness effects in the N -body problem should be viewed very differently from the chaos associated with a bulk, possibly nonintegrable, potential. More recently Di Cintio & Casetti (2019) studying test orbits in live direct N -body simulations with N up to $\approx 10^5$ reached similar conclusions. In particular (see their figs. 7 and 12) the weak scaling of orbital chaoticity with the number of degrees of freedom (i.e. number of particles at fixed normalization) has a different trend for different energies.

For what concerns the largest Lyapunov exponent λ_{\max} of the full N -body problem, whereas some studies suggest that it increases for increasing N (see Goodman et al. 1993; Hemsendorf & Merritt 2002; Portegies Zwart et al. 2022; Portegies Zwart & Boekholt 2023), some others (Beraldo e Silva et al. 2019; Di Cintio & Casetti 2019, 2020) indicate instead that λ_{\max} is inversely proportional to N , at least for $N \gtrsim 10^4$, as suggested by the semi-analytical estimation of Gurzadyan & Savvidy (1986) and Gurzadyan & Kocharyan (2009). These manifestly contradicting findings are currently not yet reconciled. The use or not of a regularized version of the Coulombian $1/r$ potential, such as for example the usual $1/\sqrt{r^2 + \epsilon^2}$ can only partially explain while models with softened interactions have systematically lower Lyapunov exponents due to the absence of hard scattering events¹ among particles. Moreover, convergence studies at

¹ We note that, Gurzadyan & Savvidy (1986) when evaluating their $\lambda_{\max} \propto N^{-1/3}$ relation imposed a cut-off on the tail of the stochastic force

fixed system parameters with decreasing values of the softening length ϵ , yield similar values of the Lyapunov exponents below some critical ϵ (see fig. 2 of Kandrup & Sideris 2001 and fig. 6 of Di Cintio & Casetti 2019).

These apparently conflicting results indicate that the use of the Lyapunov exponent alone might not be enough to characterise chaos in gravitational N -body systems. Of course, up to this point we have discussed the largest λ . The full spectrum may differ substantially between realizations with different N and similar λ_{\max} . For example Di Cintio & Trani (2025) showed that in the three-body problem with relativistic corrections included in the force calculations, the largest Lyapunov exponents can be comparable to (or even smaller than) their classical counterparts, while the full spectrum may differ significantly between the two cases.

It is therefore worth exploring other metrics of chaos in addition to the Lyapunov exponents and related quantities such as the small alignment indexes (SALI, Skokos 2001); generalized alignment indexes (GALI, Skokos et al. 2007) or the mean exponential growth factor of nearby orbits (MEGNO, Cincotta & Simó 2000; Mestre et al. 2011). For example, several studies in the context of simple dynamical systems (e.g. see Chernov 1997; Papenbrock 2000; Shiozawa & Tokuda 2024) used the Kolmogorov-Sinai (KS, Kolmogorov 1958, 1959; Sinai 1959) entropy \mathcal{S}_{KS} (see Lichtenberg & Leiberman 1992). Once a coarse graining of time and phase-space is defined, the KS entropy quantifies the rate of information production along a trajectory, as inferred from the conditional probabilities that the trajectory occupies a given phase-space cell j at time t_{n+1} given its history up to time t_n . Remarkably, Pesin (1977) found that for Hamiltonian systems, the KS entropy is bounded from above by the sum of the positive Lyapunov exponents,

$$\mathcal{S}_{\text{KS}} \leq \mathcal{S}_{\text{KS}}^+ = \sum_{\lambda_i > 0} \lambda_i. \quad (5)$$

Another commonly used entropy measure is the Shannon information entropy (Shannon & Weaver 1949). Given a partition of phase space into cells k , with occupation probabilities $p_k(t)$ (e.g. estimated from an ensemble of trajectories at a fixed time t), the Shannon entropy is

$$\mathcal{S}_{\text{Sh}}(t) = - \sum_k p_k(t) \ln p_k(t), \quad (6)$$

and quantifies how broadly the ensemble is distributed over the chosen coarse-grained representation. The Shannon and KS entropy are conceptually similar in that both depend on coarse graining and capture information content. However, $\mathcal{S}_{\text{Sh}}(t)$ is an instantaneous property of a probability distribution (and may be tracked in time if the distribution evolves), whereas \mathcal{S}_{KS} is an asymptotic entropy rate associated with the time evolution of a single trajectory, defined from the statistics of sequences of its visits in phase space cells.

The use of entropy-based quantities as indicators of relaxation and dynamical chaos has been rather successful in celestial mechanics. In a series of studies (Núñez et al. 1996; Cincotta et al. 1999; Giordano & Cincotta 2018; Cincotta et al. 2021), the information entropy was employed to quantify the dynamical stability of ensembles of trajectories in the restricted three-body problem and to identify periodic and chaotic patterns in astronomical data.

distribution acting on each test mass, de facto corresponding to softening the gravitational interaction below a fixed scale length (D.Heggie, private communication).

These diagnostics are complementary to frequency map analysis, which instead characterizes orbital regularity through the Fourier decomposition of time series and the (in)stability of the associated fundamental frequencies. Frequency map analysis was originally introduced in planetary dynamics (Laskar 1990) and later widely adopted in accelerator beam dynamics (Shatilov et al. 2011). More recently, Hyman et al. (2025) introduced a framework for orbital-complexity analysis based on permutation entropy and statistical complexity measures, while Canbaz (2025) proposed a novel indicator called permutation entropy of the power spectrum, which combines elements of permutation entropy with Fourier-based analysis.

In this work, we investigate the relationship between different chaos indicators by comparing the maximal Lyapunov exponent and the Shannon entropy in two idealised systems: a test particle in the Hénon-Heiles potential and in the potential generated by N particles distributed according to a Plummer profile. We assess the degree to which these indicators yield consistent classifications of regular and chaotic dynamics, and identify regimes in which their interpretations diverge. We also examine the dependence of these indicators on the particle number N , with the aim of clarifying the apparently contradictory results on the relation between chaoticity and the number of degrees of freedom in the N -body problem.

The rest of the paper is structured as follows: In Sect. 2 we introduce the governing equations, we discuss the numerical integration and describe the procedure to evaluate the Lyapunov exponents and the information entropy. In Sect. 3 we present our numerical simulations and discuss the results. Finally, in Sect. 4 we draw our conclusions and interpret our findings in the light of previous work.

2. Methods

2.1. Models

In this work, we consider two models, specifically, the Hénon & Heiles (1964) (hereafter HH) system, and a spherical N -body system in which the motion of a single particle is studied within the time-dependent gravitational potential generated by the remaining $N - 1$ particles

2.1.1. Hénon-Heiles system

The HH system is defined by the Hamiltonian

$$\mathcal{H}_{\text{HH}} = \frac{p_x^2 + p_y^2}{2} + \frac{x^2 + y^2}{2} + x^2 y - \frac{y^3}{3}, \quad (7)$$

and was originally conceived as a toy model for the dynamics in the meridional plane of an axisymmetric galactic potential. It has since become a paradigmatic example in nonlinear dynamics, exhibiting a mixed phase space, i.e. a nontrivial coexistence of regular and chaotic orbits on the same energy surface (Weiss et al. 2003). Here, we adopt the conventional rescaling in which the particle mass m and the coefficients of all terms in the two-dimensional potential are set to unity. With this normalization, the critical energy above which all trajectories escape is $E_{\text{crit}} = 1/6$. The equations of motion derived by Eq. (7) and the associated variational equations, defined by Eq. (3), read

$$\ddot{x} = -x - 2xy \quad (8)$$

$$\ddot{y} = -x^2 + y^2 - y \quad (9)$$

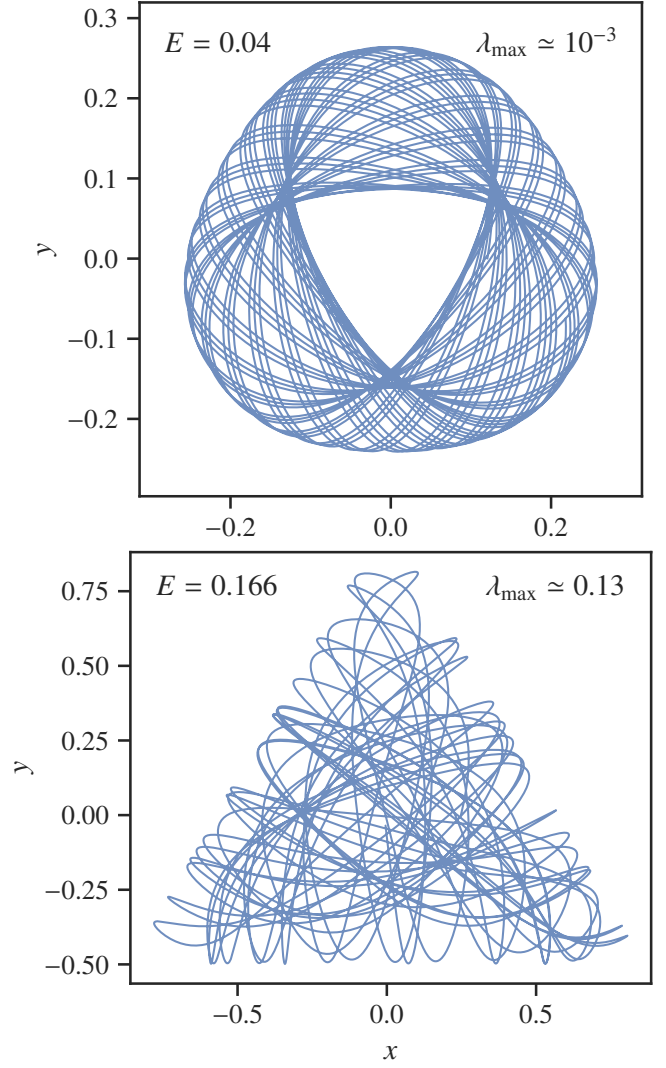


Fig. 1. Illustration of two trajectories in the HH system. Top panel: low-energy, regular trajectory with nearly-zero maximal Lyapunov exponent λ_{max} . Bottom panel: high-energy, chaotic trajectory with finite λ_{max} .

and

$$\delta\dot{x} = -(1 + 2y)\delta x - 2x\delta y \quad (10)$$

$$\delta\dot{y} = -2x\delta x - (1 - 2y)\delta y, \quad (11)$$

respectively. Figure 1 illustrates a typical regular and chaotic orbit in the the HH system, corresponding to $E = 0.04$ and $E = 0.16$.

2.1.2. N -body system

We probe the dynamics of individual orbits in spherical equilibrium self gravitating N -body models evolving test particles in the time-dependent gravitational potential exerted by the remaining $N - 1$ bodies. The equation of motion for the i -th particle of mass m is

$$\ddot{\mathbf{r}}_i = -Gm \sum_{i \neq j=1}^N \frac{\mathbf{r}_i - \mathbf{r}_j}{r_{ij}^3}, \quad (12)$$

where G is the gravitational constant and $r_{ij} = \|\mathbf{r}_i - \mathbf{r}_j\|$. The associated variational equations in tangent space, required for the

computation of Lyapunov exponents (see, e.g., Rein & Tamayo 2016), read

$$\ddot{\delta\mathbf{r}}_i = -Gm \sum_{\substack{j=1 \\ j \neq i}}^N \left[\frac{\delta\mathbf{r}_i - \delta\mathbf{r}_j}{r_{ij}^3} - 3(\mathbf{r}_i - \mathbf{r}_j) \frac{\langle \delta\mathbf{r}_i - \delta\mathbf{r}_j, \mathbf{r}_i - \mathbf{r}_j \rangle}{r_{ij}^5} \right]. \quad (13)$$

In the N -body experiments, the initial positions and velocities of the N particles are drawn from the widely adopted Plummer (1911) model, with total mass M and scale radius a , and defined by the following spherical density-potential pair:

$$\rho(r) = \frac{3M}{4\pi a^3} \left(1 + \frac{r^2}{a^2}\right)^{-5/2}; \quad \Phi(r) = -\frac{GM}{\sqrt{r^2 + a^2}}, \quad (14)$$

supported by the ergodic phase-space distribution function

$$f(E) = \frac{\sqrt{2}}{378\pi^2 G a^2 \sigma_0} \left(\frac{-E}{\sigma_0^2}\right)^{7/2}. \quad (15)$$

Here E denotes the specific energy of a particle and $\sigma_0 = \sqrt{GM/6a}$ is the central velocity dispersion. All quantities are expressed in N -body units, such that $G = M = a = 1$ and each particle has equal mass $m = M/N$. Consequently, the typical crossing time $t_c \equiv \sqrt{a^3/GM} = 1$. We simulate different sets of initial conditions with N between 10^4 and 10^6 . As N increases, the total mass is held fixed, consequently, the individual particle mass decreases accordingly.

We approximate the dynamics by evolving $N - 1$ independent ‘‘field’’ particles in the smooth potential (14), while computing the trajectory and associated tangent dynamics of a ‘‘test’’ particle according to Eqs. (12–13). In this framework, the variational vectors of the field particles, $\delta\mathbf{r}_j$, evolve in the Plummer potential according to

$$\ddot{\delta\mathbf{r}}_j = -Gm \left[\frac{\delta\mathbf{r}_j}{(r_j^2 + a^2)^{3/2}} - 3\mathbf{r}_j \frac{\langle \delta\mathbf{r}_j, \mathbf{r}_j \rangle}{(r_j^2 + a^2)^{5/2}} \right]. \quad (16)$$

2.2. Numerical integration

For both the HH system and the N -body system, we integrate the equations of motion, Eqs. (8) and (12), together with their associated variational equations (Skokos & Gerlach 2010), using the fourth-order symplectic integration scheme discussed in Laskar & Robutel (2001, see also Yoshida 1990, 1993; Kinoshita et al. 1991 and references therein). In all runs, we adopt a fixed timestep Δt that depends on the initial orbital energy. The timestep is determined through preliminary trial-and-error integrations, requiring that over an integration time of 5×10^3 time units the relative energy error remains below 10^{-9} in double precision for the HH system. In the N -body runs, for the dimensionless equations of motion considered here, the resulting optimal timesteps typically lie in the range $2 \times 10^{-5} \leq \Delta t \leq 10^{-2}$. As we are following individual test trajectories in time dependent N -body potentials, we do not employ any softening or regularization of the gravitational interactions.

2.3. Evaluation of the Lyapunov exponents

Evaluating the maximal Lyapunov exponent of a given system by simply time-dependently computing (1) up to a desired convergence is typically unfeasible as it is in principle plagued by round-off errors resulting in a rapid blow-up of the numerical

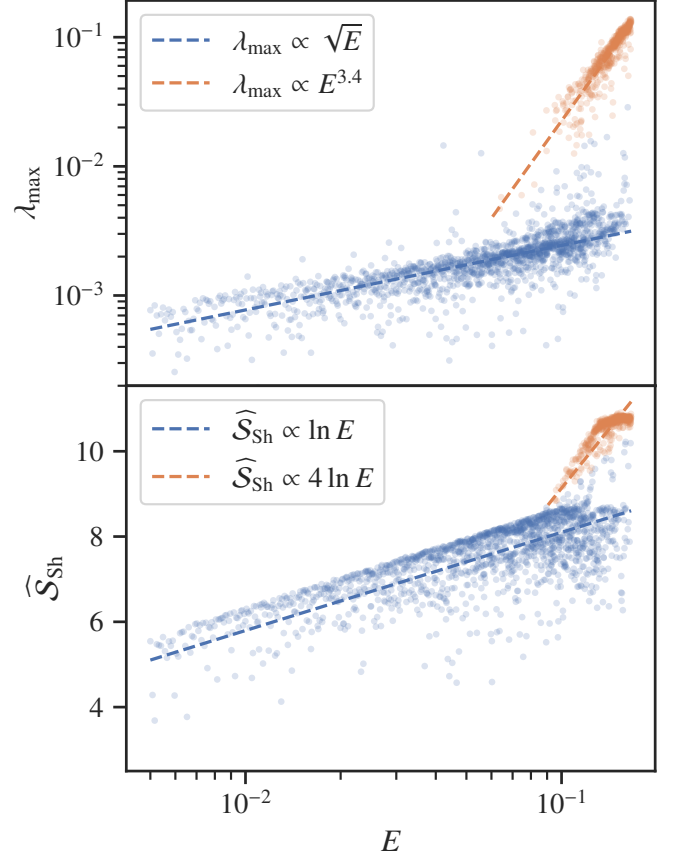


Fig. 2. Maximal Lyapunov exponent λ_{\max} (top panel) and Shannon entropy \widehat{S}_{Sh} (bottom panel) versus energy for 2000 realizations of the HH system. In the top panel, the blue and red dashed lines mark the trends $\lambda_{\max} \propto \sqrt{E}$ and $\lambda_{\max} \propto E^{3.4}$ reported by Shevchenko & Mel’nikov (2003). In the bottom panel, the curves $\widehat{S}_{\text{Sh}} \propto \ln E$ and $\widehat{S}_{\text{Sh}} \propto 4 \ln E$ are shown for comparison. Both λ_{\max} and \widehat{S}_{Sh} increase with energy, with a change in slope around $E \simeq 0.08$, marking the transition from predominantly regular to chaotic trajectories.

solution. Following Benettin et al. (1976) in the numerical calculations we obtain λ_{\max} as the limit of

$$\lambda_{\max}(t) = \frac{1}{L\Delta t} \sum_{k=1}^L \ln \frac{\|\mathbf{W}(k\Delta t)\|}{\|\mathbf{W}_0\|}, \quad (17)$$

for a (large) time $t = L\Delta t$ with the additional precaution of periodically re-normalizing \mathbf{W} to its initial magnitude (see e.g. Skokos 2010 and references therein). When computing λ_{\max} for an individual particle in N -body experiments, we also average over different experiments where the other $N - 1$ background particles are sampled from the same model in a similar fashion to what done in Sartorello et al. (2025) for particles in time-dependent gravitational potential subjected to noise.

2.4. Information entropy

We compute the information entropy in two distinct ways. First, for individual orbits we evaluate Eq. (6) from the empirical phase-space density in the full state vector $(x, y, p_x, p_y)(t)$, obtained by coarse-graining the trajectory samples into a multidimensional histogram. Denoting by \hat{p}_k the fraction of stored sam-

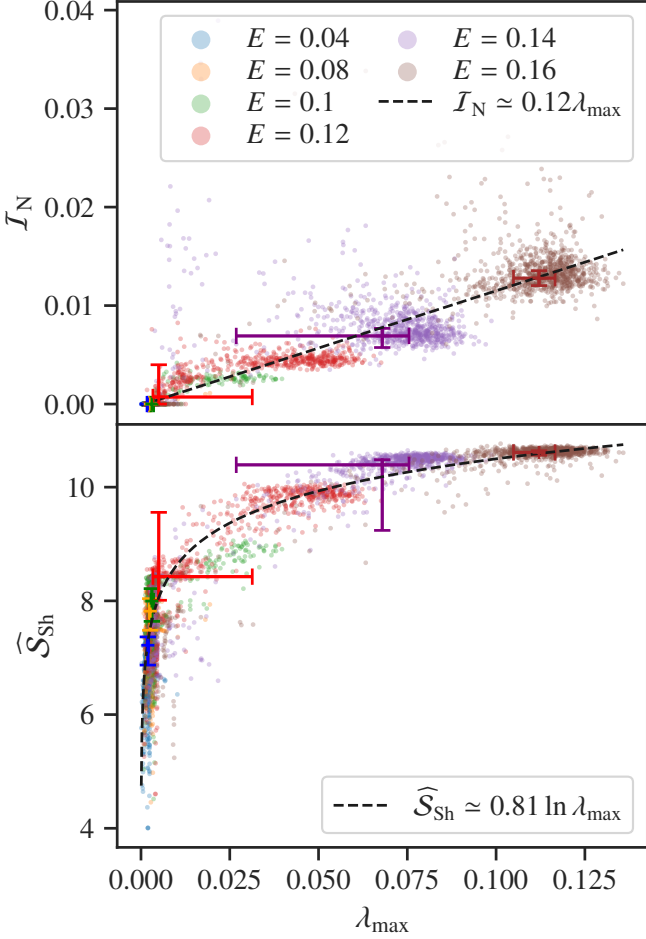


Fig. 3. Average mutual information entropy I_N (top panel) and Shannon entropy (bottom panel) versus the maximal Lyapunov λ_{\max} for different values of the energy E in the range $0.04 \leq E \leq 0.16$ in the HH system. Error bars indicate the 1σ scatter over the ensemble, shown by the coloured points. In both panels, dashed lines represent the best-fitting relation between the entropy and λ_{\max} .

ples that fall in bin k , our estimator is

$$\widehat{S}_{\text{Sh}} \equiv - \sum_k \hat{p}_k \ln \hat{p}_k, \quad (18)$$

where the sum runs over all bins (with the convention that empty bins contribute zero). To mitigate the dependence on an arbitrary bin choice, we estimate a reference bin width in each coordinate using the Freedman-Diaconis rule, and then scan a range of nearby binnings to verify the stability of the inferred entropy. We enforce a minimum sampling quality by requiring an average occupancy of at least five samples per non-empty bin, i.e. $N_{\text{samp}}/N_{\text{occ}} \geq 5$, where N_{samp} is the number of stored phase-space samples and N_{occ} is the number of occupied bins. For consistent entropy comparisons, a common binning is adopted for all trajectories within a given comparison set. We also explored nearby binning configurations, and verified that the qualitative trends, and the quantitative values within uncertainties, remain unchanged. In this definition, \widehat{S}_{Sh} quantifies how broadly the trajectory populates the accessible phase space (at the chosen coarse-graining), and is therefore a measure of phase-space exploration rather than of instantaneous information-production rate.

Second, we evaluate the mutual information entropy introduced by Núñez et al. (1996, see also Fraser & Swinney 1986), which we denote with I_N . Although its formal definition resembles that of a mutual-information Shannon entropy, the quantity I_N is not a mutual information in the probabilistic sense. Instead, it is constructed by calculating the Shannon entropy of normalized arc-length weights along two trajectories in phase space, and by combining the resulting entropies in a way that is sensitive to the dynamical decorrelation between nearby realizations. Given a reference trajectory $\xi(t)$ and a nearby realization $\xi'(t)$ initialized at separation $\|\xi'(0) - \xi(0)\| = d_0$, Núñez et al. (1996) define

$$I_N(t) = \mathcal{S}_N(\xi, \xi'; t) - \frac{1}{2} [\mathcal{S}_N(\xi; t) + \mathcal{S}_N(\xi'; t)], \quad (19)$$

where the entropies are computed from normalized path-length rates along the curves. For a single trajectory $\xi(t)$, we define the instantaneous speed in phase space,

$$\dot{\ell}_\xi(t) = \|\dot{\xi}(t)\|, \quad (20)$$

the accumulated path length up to time t ,

$$L_\xi(t) = \int_0^t \dot{\ell}_\xi(t') dt', \quad (21)$$

and the corresponding normalized length density

$$\varepsilon_\xi(t) = \frac{\dot{\ell}_\xi(t)}{L_\xi(t)} \quad (22)$$

The path-length entropy for an individual trajectory is then the Shannon entropy of this time-density,

$$\mathcal{S}_N(\xi; t) = - \int_0^t \varepsilon_\xi(t') \ln \varepsilon_\xi(t') dt'. \quad (23)$$

For the joint entropy estimator $\mathcal{S}_N(\xi, \xi'; t)$, one defines

$$\dot{\ell}_{\xi\xi'}(t) = \sqrt{\dot{\ell}_\xi^2(t) + \dot{\ell}_{\xi'}^2(t)}, \quad (24)$$

$$L_{\xi\xi'}(t) = \int_0^t \dot{\ell}_{\xi\xi'}(t') dt', \quad (25)$$

$$\varepsilon_{\xi\xi'}(t) = \frac{\dot{\ell}_{\xi\xi'}(t)}{L_{\xi\xi'}(t)}, \quad (26)$$

and substitutes $\varepsilon_{\xi\xi'}$ into Eq. (23) to obtain $\mathcal{S}_N(\xi, \xi'; t)$. In contrast to \widehat{S}_{Sh} , $I_N(t)$ is sensitive to dynamical divergence: as the perturbed trajectory deviates from the reference one, the joint and marginal length densities evolve differently, producing a characteristic growth and eventual saturation of $I_N(t)$ in chaotic regimes (Núñez et al. 1996). In this sense, I_N plays a role analogous to that of a Lyapunov exponent as a diagnostic of instability, while remaining a finite-time quantity. A practical distinction is that the mutual information entropy as defined by Núñez et al. (1996) cannot, in general, be computed from tangent-vector dynamics alone: its definition depends on the accumulated path length of a genuinely distinct trajectory, which is not preserved under the renormalization steps required by the Lyapunov-exponent computation algorithm.

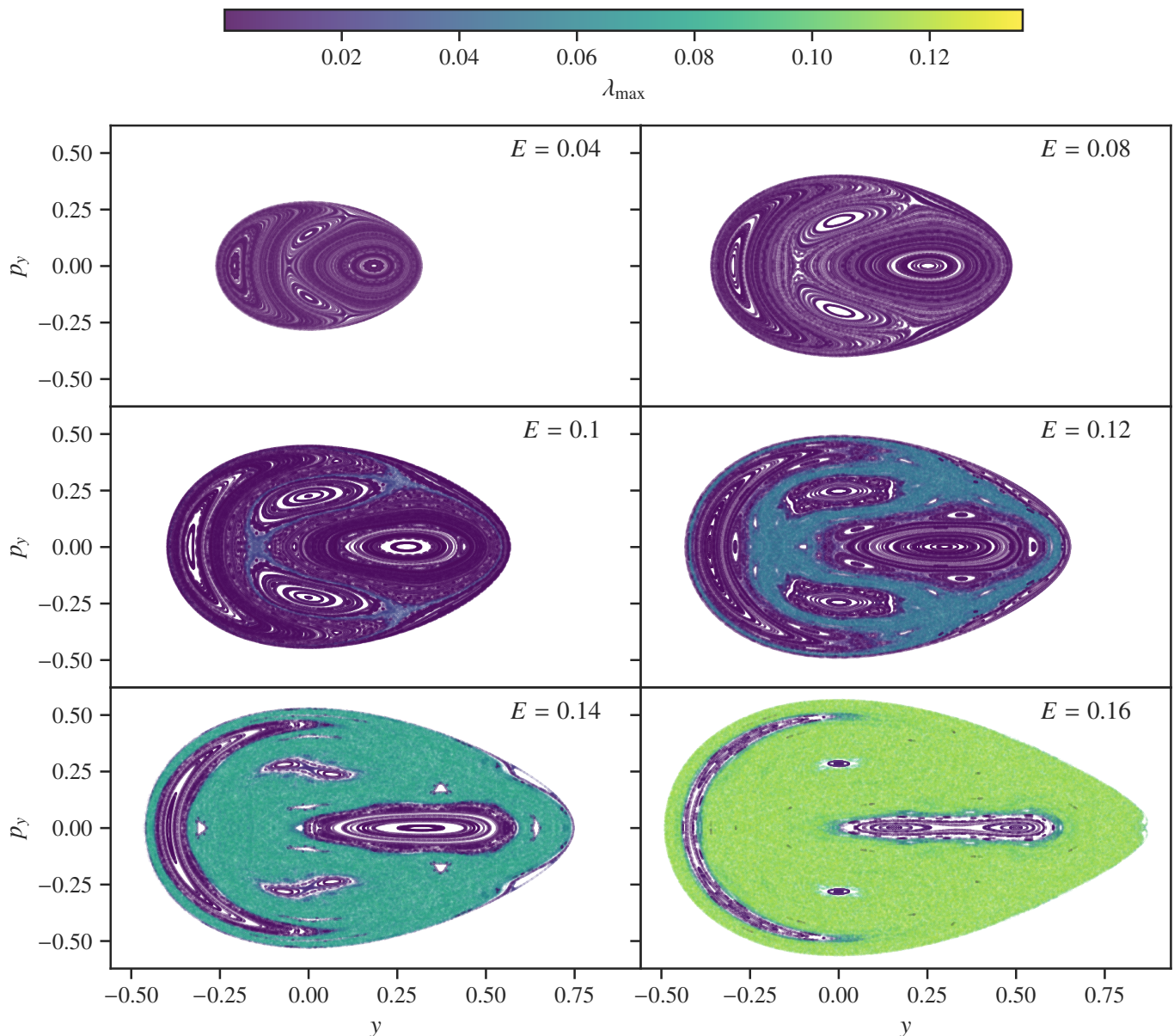


Fig. 4. Poincaré sections (y, p_y) of the HH Hamiltonian for different values of the energy E , defined by crossings of the plane $x = 0$. The colour coding represents the maximal Lyapunov exponent λ_{\max} of the orbits.

3. Numerical experiments and results

3.1. HH system

It is well known that in the HH potential the maximal Lyapunov exponent λ_{\max} , averaged over an energy surface, increases with E . Early computations by Benettin et al. (1976) suggested an $\exp E$ trend for both λ_{\max} and the KS entropy S_{KS} . Subsequent studies, for example Shevchenko & Mel'nikov (2003), instead reported a broken power-law trend, with a sharp change in slope at $E \approx 0.08$ for the averaged Lyapunov exponent.

In the energy range $10^{-3} \leq E < 1/6$ we evaluate both the maximal Lyapunov exponent and the Shannon entropy on a grid of 10^3 realizations. The top panel of Figure 2 shows λ_{\max} as a function of orbital energy E . Orange and blue points highlight the two regimes, indicated by the corresponding dashed lines, where $\lambda \propto \sqrt{E}$ and $\lambda \propto E^{3.4}$, respectively. The Shannon entropy \widehat{S}_{Sh} for the same orbits is shown in the bottom panel, and like-

wise exhibits a broken trend with E , consistent with $\widehat{S}_{\text{Sh}} \propto \ln E$ for $E \lesssim 0.08$ and $\widehat{S}_{\text{Sh}} \propto \ln E^4$ for $E \gtrsim 0.08$. Note that, in principle, for a given value of E , due to the coexistence of wildly chaotic and nearly regular orbits, the values of the Lyapunov exponents for different trajectories can differ significantly, resulting in highly non-trivial distributions $P(\lambda)$ (e.g. Vallejo et al. 2008).

In Figure 3 we present the mutual information entropy \mathcal{I}_N (top panel) in addition to the Shannon entropy \widehat{S}_{Sh} (bottom panel) against the mean Lyapunov exponent. We find that \mathcal{I}_N scales linearly with λ_{\max} while the Shannon entropy is compatible with a $\widehat{S}_{\text{Sh}} \propto \ln \lambda_{\max}$ relation, in agreement with the picture emerging from Figure 2.

The correspondence between the mutual information entropy and the Lyapunov exponent can be visualized by colour-coding these indicators in the Poincaré sections of the trajectories at fixed values of E . In Figures 4 and 5, we show the sections in (y, p_y) defined by $x = 0$, colour-coded by λ_{\max} and \mathcal{I}_N , respec-

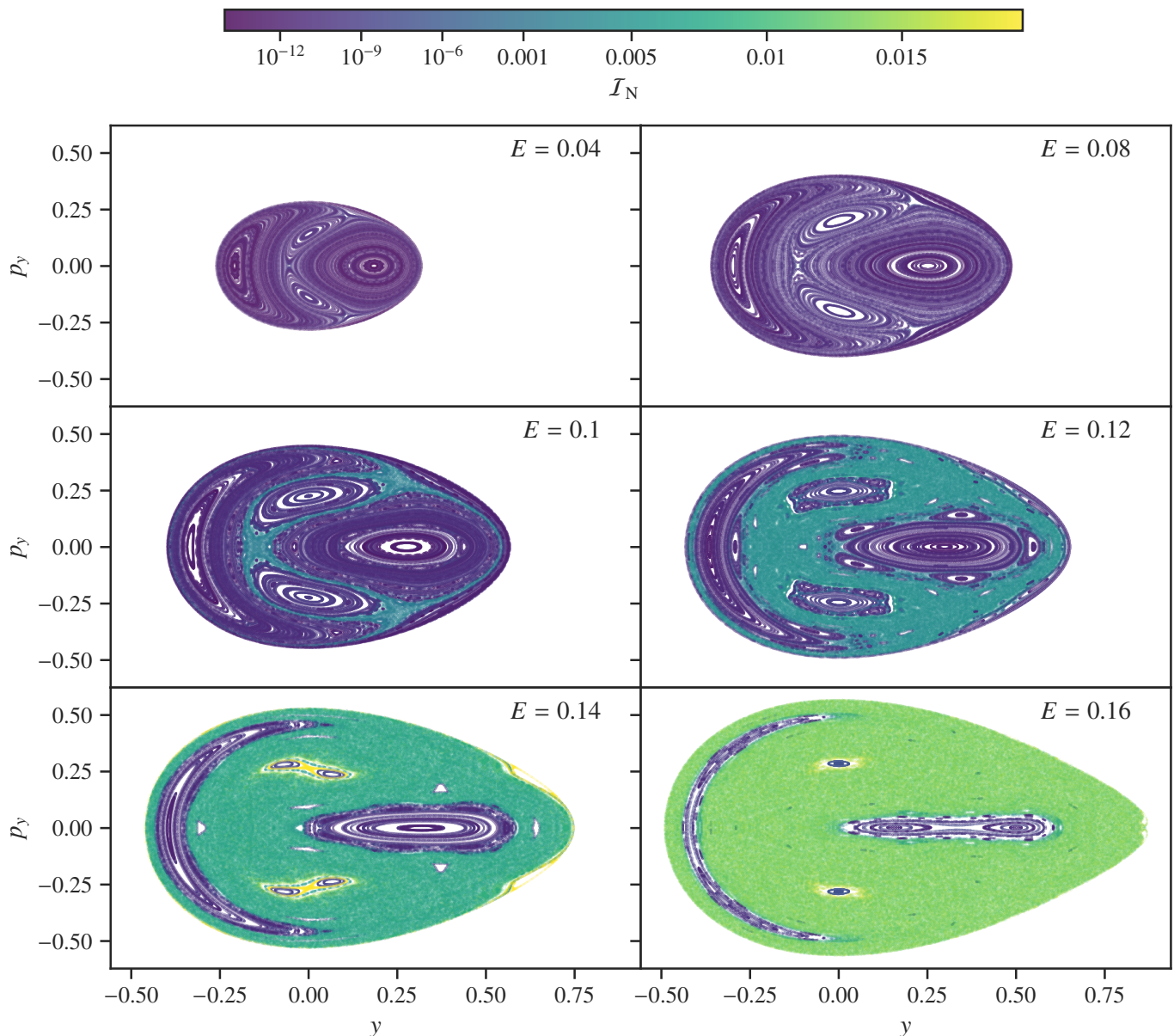


Fig. 5. Poincaré sections (y, p_y) of the HH Hamiltonian for different values of the energy E , defined by crossings of the plane $x = 0$. The colour coding represents the mutual information entropy \mathcal{I}_N (Eq. 19) of the orbits.

tively, for different energies. Both indicators, despite the greater scatter of \mathcal{I}_N at nearly equal λ_{\max} , reveal how for $E \gtrsim 0.8$ the fraction of accessible phase-space is indeed occupied by a rapidly growing fraction of chaotic orbits though with a persistent measure of regular islands, even for the $E = 0.16$, closer to the $E = 1/6$ threshold case.

3.2. N -body models

We performed a series of N -dependent numerical experiments on test orbits for different values of the initial particle energy. As mentioned above, numerical studies on frozen N -body realizations of simple galactic potentials (see e.g. Kandrup & Sideris 2001; Sideris & Kandrup 2002; Kandrup et al. 2004) seem to suggest that individual particle trajectories, for increasing N approach more and more closely their counterparts in the parent smooth system, while their largest Lyapunov exponent does not

show a significant decreasing trend with N , as one would naively expect.

In the range $10^4 \leq N \leq 10^6$, we observe a similar tendency even in our time-dependent N -body potentials for the orbits of test particles initialized with exactly the same phase space position approaches in realizations of the potential with increasing values of N . As an example, in Figure 6 we show the trajectory for a particle of initial energy per unit mass $E \approx -0.66$ in Plummer models sampled by $N = 10^4, 3 \times 10^4, 10^5, 3 \times 10^5$ and 10^6 . Notably, as N increases the fluctuations of the orbital inclination become less and less important, being already negligible for $N = 10^6$. A similar behaviour is observed for other values of the orbital eccentricity and initial energy (not shown here), with highly eccentric orbits at fixed E (i.e. having lower values of angular momentum) being generally more subjected to wild fluctuations in the inclination, even at $N \approx 10^5$.

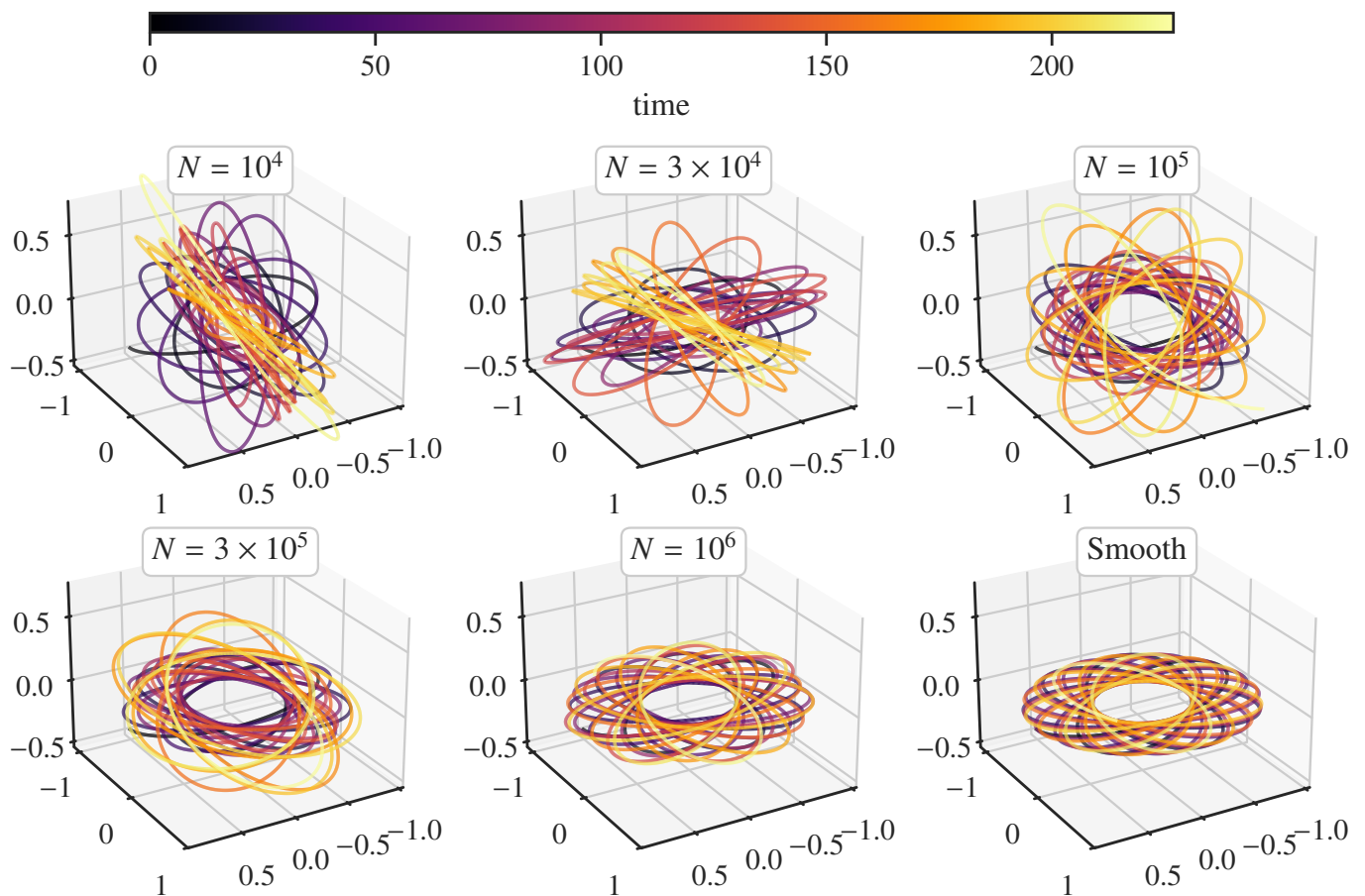


Fig. 6. Tracer particle orbit with initial energy $E \approx -0.66$ in different N -body realizations of an isotropic Plummer model with increasing N , and in the smooth-potential (continuum) limit. The colour coding represents time in units of t_c . As N increases, the orbit approaches its continuum counterpart.

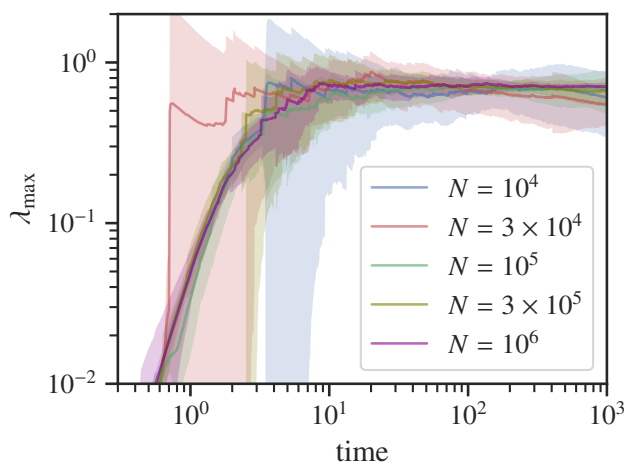


Fig. 7. Evolution of the maximal Lyapunov exponent λ_{\max} for different values of N in the N -body system. Solid lines show the mean over 10 realizations, and the shaded regions indicate the 1σ dispersion.

We note that λ_{\max} evaluated as function of a given value of the energy E depends weakly on N (see also fig. 2 in Kandrup & Sideris 2001, fig. 12 in Di Cintio & Casetti 2019 and fig. 10 in Sartorello et al. 2025). This is evidenced in Figure 7 where we

tracked the evolution of the mean finite time largest Lyapunov exponent for the same orbital initial condition (i.e. test particle with equal combinations of \mathbf{r} and \mathbf{v}), propagated in different realizations of the Plummer model at different values of N . Using the same number of independent samplings of the underlying model (shaded areas) the mean values of λ_{\max} over the ensemble relax to comparable values over 10^3 dynamical times, regardless of N .

We emphasise that, unlike in the frozen-potential experiments of Kandrup and collaborators, the energy of the test particle is not conserved for any N , owing to the time-dependent potential generated by the N moving field particles. It is therefore necessary to quantify the range of energies explored along each trajectory.

In the top panel of Figure 8 we show λ_{\max} as a function of the median energy over the full integration. Orbits at lower energies (i.e. particles deep in the potential well) have larger values of their largest Lyapunov exponent, whereas the orbits exploring higher energies (i.e. weakly bound particles) systematically show smaller λ_{\max} . This trend is consistent with the relation between the averaged λ_{\max} and the initial energy found in noisy-potential experiments mimicking an increasing number of field particles (up to 10^{13}) by Sartorello et al. (2025), as well as in low-resolution direct N -body simulations by Di Cintio & Casetti (2019). Furthermore, as N increases, the scatter in λ_{\max} about its relation with the median energy decreases.

Because particle energy is not conserved, we compare λ_{\max} against both the initial and median energy at fixed N . As shown

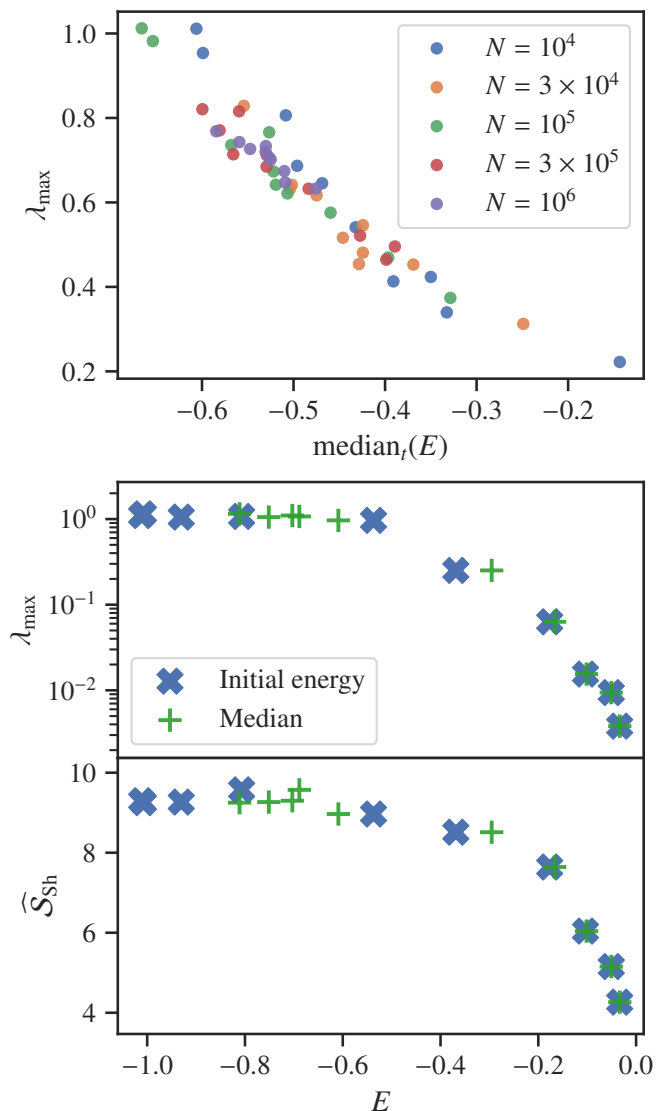


Fig. 8. Top panel: maximal Lyapunov exponent λ_{\max} versus the orbital energy E of the test particle in the N -body system, where E is taken as the median along the trajectory. Colors indicate the number of particles N . Lower panels: λ_{\max} (upper sub-panel) and Shannon entropy \widehat{S}_{Sh} (lower sub-panel) versus the initial (blue crosses) and median (green crosses) orbital energy in a realization of an isotropic Plummer model at fixed $N = 10^5$. Both λ_{\max} and \widehat{S}_{Sh} decrease with increasing orbital energy and approach a saturation level for the most tightly bound orbits.

in the lower panels of Figure 8, both λ_{\max} and \widehat{S}_{Sh} decreases monotonically with both quantities. Notably, for weakly bound particles ($E \gtrsim -0.3$), the initial and median energies (green crosses) are nearly identical, as expected for orbits confined to the lower-density outskirts of the cluster.

With this established, the top and middle panels of Figure 9 show violin plots of λ_{\max} and the information entropy \widehat{S}_{Sh} , respectively, including their statistical spread, for orbits with initial energy $E = -0.45$ (corresponding to a circular orbit of radius a in the smooth Plummer potential). The orbits are evolved across ensembles of discrete realizations with increasing N .

The distribution of the largest Lyapunov exponent shows no significant dependence on N over this range, while its spread narrows markedly with increasing N . The lower envelope of λ_{\max} is

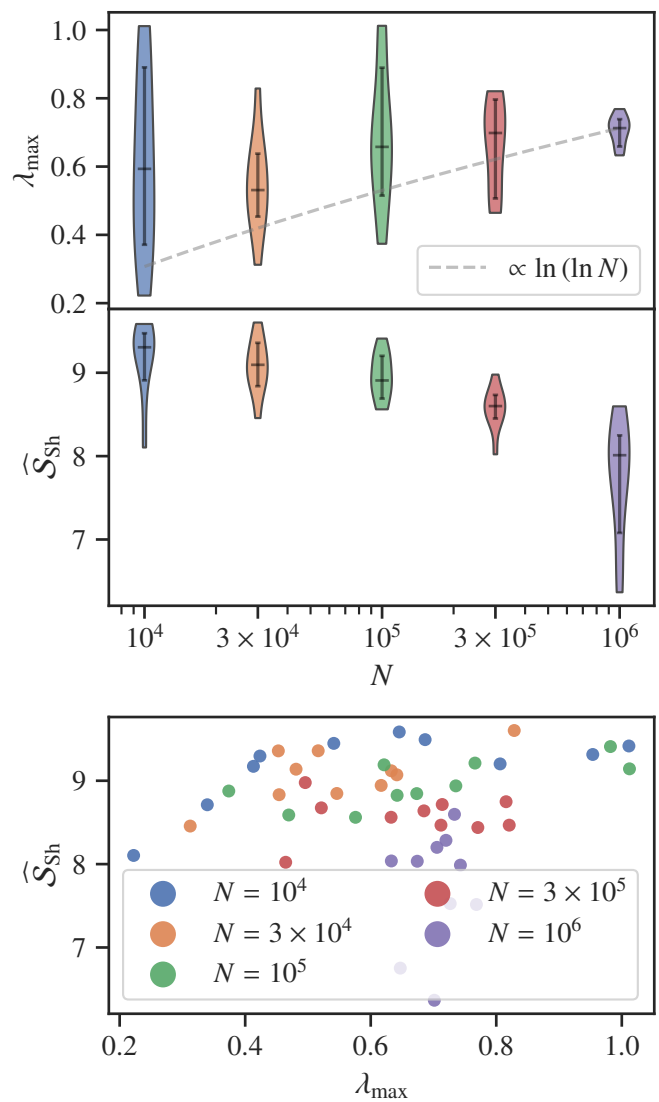


Fig. 9. Upper panels: distributions of the maximal Lyapunov exponent λ_{\max} (upper sub-panel) and Shannon entropy \widehat{S}_{Sh} (lower sub-panel) for different values of N in the N -body system. Error bars indicate the median and the associated 1σ scatter. In the upper sub-panel, the dashed line denotes the scaling proposed by Goodman et al. (1993). Bottom panel: \widehat{S}_{Sh} versus λ_{\max} for individual realizations of the N -body system. The maximal Lyapunov exponent shows no significant dependence on N , whereas the Shannon entropy decreases with increasing N .

broadly consistent with the $\ln(\ln N)$ scaling proposed by Goodman et al. (1993). In contrast, the entropy decreases with N and exhibits a broader spread, particularly at $N \sim 10^6$. This trend is also evident in the bottom panel, which shows \widehat{S}_{Sh} as a function of λ_{\max} for individual realizations. At fixed N , larger Lyapunov exponents are broadly associated with higher entropy, although the correlation is weaker than in the HH system.

4. Discussion and conclusions

We have investigated the relation between the largest Lyapunov exponent and different formulations of information entropy in the paradigmatic Hénon & Heiles (1964) 2D potential and for individual particle orbits in time-dependent N -body potentials. Our main results can be summarized as follows.

For the HH model, the Shannon entropy averaged over trajectories on the same energy surface scales logarithmically with energy, with different pre-factors in the ≤ 0.08 and ≥ 0.08 regimes (Figure 2). This change in prefactor reflects the transition from weakly to strongly chaotic motion across the well known onset of widespread chaos in the HH system. This behaviour is consistent with that of the largest Lyapunov exponent and of the mutual information entropy. The latter scales approximately linearly with λ_{\max} , whereas \widehat{S}_{Sh} exhibits a logarithmic dependence (Figure 3).

For single-particle orbits in N -body realizations of a given gravitational potential (here, a spherical Plummer model), λ_{\max} is larger for more tightly bound orbits (i.e. lower energies), while it decreases for less bound trajectories; the same qualitative trend is observed for the Shannon entropy (Figure 8). At fixed initial conditions, increasing the resolution of the N -body system (i.e. larger N at fixed total mass) produces little variation in λ_{\max} , even as the dynamics approaches the continuum limit (Figure 9). In contrast, the Shannon entropy decreases monotonically with N , largely independently of E , in qualitative agreement with frequency-map analyses of frozen N -body systems (Kandrup & Sideris 2001; Sideris & Kandrup 2002). This discrepancy suggests that λ_{\max} alone is not a sufficient indicator of chaoticity in gravitational N -body systems. Being related to the KS entropy, i.e. to the sum of the positive Lyapunov exponents, \widehat{S}_{Sh} appears to provide a more informative diagnostic, although it relies on coarse-graining and finite-time sampling.

We conjecture that, as N increases, $\lambda_1 \equiv \lambda_{\max}$ remains approximately constant (at least up to $N = 10^6$), while the second and third exponents λ_2 and λ_3 decrease significantly beyond $N \sim 10^5$. This interpretation is supported by Figure 6 ($N = 10^6$), where perturbations in the precession frequency persist, but fluctuations of the orbital plane are strongly suppressed, indicating near conservation of angular momentum. We note that, in a related context, the inclusion of post-Newtonian corrections can decrease the leading exponent while increasing subdominant ones in certain configurations of the three-body problem (Di Cintio & Trani 2025).

A direct test would require computing the full Lyapunov spectrum (Eq. 4) for the test particle. However, this entails orthonormalization in a $6N$ -dimensional phase space, which requires evolving and orthonormalizing a $6N \times 6N$ tangent basis and becomes computationally prohibitive already at $N \approx 10^4$. An alternative is to track the deformation of an initially hyperspherical ensemble of trajectories, as proposed by Sartorello et al. (2025).

In light of these results, we speculate that the N -body chaos driven by close encounters (sometimes referred to as punctuated chaos, see Portegies Zwart et al. 2023; Boekholt et al. 2023) which appears to increase with N (Portegies Zwart & Boekholt 2023), primarily reflects the behaviour of the largest Lyapunov exponent, which probes local instability driven by close encounters, rather than global phase-space transport. In contrast, a dynamical entropy measure, being sensitive to global mixing through the full Lyapunov spectrum, would decrease with N , owing to the suppression of subdominant exponents. We emphasize that trajectory-based entropy measures provide a viable alternative to λ_{\max} only in low-dimensional systems (e.g. driven 1D models or 2D non-integrable potentials such as the HH system), where the sum of the positive part of the Lyapunov spectrum closely traces λ_{\max} . In higher-dimensional phase spaces, quantities such as \widehat{S}_{Sh} can instead serve as diagnostics indicating whether a full spectral analysis is required.

Finally, alternative estimates of dynamical entropy can be obtained from the compressibility of time series (e.g. from trajectory data), for instance via Lempel-Ziv-type complexity measures (Lempel & Ziv 1976; Puglisi et al. 2003). A natural extension of this work is to compare, for fixed system parameters (e.g. energy), trajectory-based entropy estimates with those derived from compression schemes. This approach may be particularly useful when variational equations are unavailable or computationally expensive, or when dealing with observational data (e.g. minor-body ephemerides or Galactic-centre S-stars), where only finite time series are accessible.

Acknowledgements. PFDC acknowledges the support from the MUR PRIN2022 project “Breakdown of ergodicity in classical and quantum many-body systems” (BECQuMB) Grant No. 20222BHC9Z. AAT and PFDC are grateful to Anna Lisa Varri and the University of Edinburgh for their hospitality during the 2nd “Chaotic rendezvous” meeting, and to the IFPU for hosting the workshop “Chaos and nonlinearity in dynamical astronomy”. AAT dedicates this work to the memory of his father, Vincenzo Trani, a mathematics teacher who inspired his interest in science. This study was completed during a period of personal recovery, and he gratefully acknowledges the support received during this time.

References

- Batygin, K. & Laughlin, G. 2008, *ApJ*, 683, 1207
- Benettin, G., Galgani, L., Giorgilli, A., & Strelcyn, J.-M. 1980, *Meccanica*, 15, 9
- Benettin, G., Galgani, L., & Strelcyn, J.-M. 1976, *Phys. Rev. A*, 14, 2338
- Beraldo e Silva, L., de Siqueira Pedra, W., Valluri, M., Sodr , L., & Bru, J.-B. 2019, *ApJ*, 870, 128
- Boekholt, T. C. N., Portegies Zwart, S. F., & Hoggie, D. C. 2023, *International Journal of Modern Physics D*, 32, 2342003
- Canbaz, B. 2025, *Journal of Korean Physical Society*, 86, 349
- Carpintero, D. D. & Aguilar, L. A. 1998, *MNRAS*, 298, 1
- Chernov, N. 1997, *Journal of Statistical Physics*, 88, 1
- Christiansen, F. & Rugh, H. H. 1997, *Nonlinearity*, 10, 1063
- Cincotta, P. M., Giordano, C. M., Alves Silva, R., & Beaug , C. 2021, *Physica D Nonlinear Phenomena*, 417, 132816
- Cincotta, P. M., Helmi, A., Mendez, M., Nunez, J. A., & Vucetich, H. 1999, *MNRAS*, 302, 582
- Cincotta, P. M. & Sim , C. 2000, *A&AS*, 147, 205
- Contopoulos, G. 2002, *Order and chaos in dynamical astronomy*
- Di Cintio, P. & Casetti, L. 2019, *MNRAS*, 489, 5876
- Di Cintio, P. & Casetti, L. 2020, *MNRAS*, 494, 1027
- Di Cintio, P. & Trani, A. A. 2025, *A&A*, 693, A53
- El-Zant, A. A., Everitt, M. J., & Kassem, S. M. 2019, *MNRAS*, 484, 1456
- Fraser, A. M. & Swinney, H. L. 1986, *Phys. Rev. A*, 33, 1134
- Giordano, C. M. & Cincotta, P. M. 2018, *Celestial Mechanics and Dynamical Astronomy*, 130, 35
- Goodman, J., Hoggie, D. C., & Hut, P. 1993, *ApJ*, 415, 715
- Gurzadyan, V. G. & Kocharyan, A. A. 2009, *A&A*, 505, 625
- Gurzadyan, V. G. & Savvidy, G. K. 1986, *A&A*, 160, 203
- Hemsendorf, M. & Merritt, D. 2002, *ApJ*, 580, 606
- H non, M. & Heiles, C. 1964, *AJ*, 69, 73
- Hyman, S. O., Daniel, K. J., & Schaffner, D. A. 2025, *ApJ*, 987, 195
- Kandrup, H. E. & Sideris, I. V. 2001, *Phys. Rev. E*, 64, 056209
- Kandrup, H. E., Sideris, I. V., & Bohn, C. L. 2004, *Physical Review Accelerators and Beams*, 7, 014202
- Kandrup, H. E. & Siopis, C. 2003, *MNRAS*, 345, 727
- Kandrup, H. E. & Smith, Haywood, J. 1991, *ApJ*, 374, 255
- Karanis, G. I. & Caranicolas, N. D. 2001, *A&A*, 367, 443
- Kinoshita, H., Yoshida, H., & Nakai, H. 1991, *Celestial Mechanics and Dynamical Astronomy*, 50, 59
- Kolmogorov, A. 1958, *Doklady Akademii Nauk SSSR*, 119, 861
- Kolmogorov, A. 1959, *Doklady Akademii Nauk SSSR*, 124, 754
- Laskar, J. 1990, *Icarus*, 88, 266
- Laskar, J. & Robutel, P. 2001, *Celestial Mechanics and Dynamical Astronomy*, 80, 39
- Lempel, A. & Ziv, J. 1976, *IEEE Transactions on Information Theory*, 22, 75
- Lichtenberg, A. & Leiberman, M. 1992, *Regular and Chaotic Dynamics*
- Mestre, M. F., Cincotta, P. M., & Giordano, C. M. 2011, *MNRAS*, 414, L100
- Milani, A. & Nobili, A. M. 1992, *Nature*, 357, 569
- Miller, R. H. 1971, *Journal of Computational Physics*, 8, 449
- Mogavero, F., Hoang, N. H., & Laskar, J. 2023, *Physical Review X*, 13, 021018
- N nez, J. A., Cincotta, P. M., & Wachlin, F. C. 1996, *Celestial Mechanics and Dynamical Astronomy*, 64, 43

- Papenbrock, T. 2000, *Phys. Rev. E*, 61, 1337
- Pesin, Y. B. 1977, *Russian Mathematical Surveys*, 32, 55
- Plummer, H. C. 1911, *MNRAS*, 71, 460
- Portegies Zwart, S. & Boekholt, T. 2023, in *American Institute of Physics Conference Series*, Vol. 2832, American Institute of Physics Conference Series (AIP), 050003
- Portegies Zwart, S. F., Boekholt, T. C. N., & Heggie, D. C. 2023, *MNRAS*, 526, 5791
- Portegies Zwart, S. F., Boekholt, T. C. N., Por, E. H., Hamers, A. S., & McMillan, S. L. W. 2022, *A&A*, 659, A86
- Puglisi, A., Benedetto, D., Caglioti, E., Loreto, V., & Vulpiani, A. 2003, *Physica D Nonlinear Phenomena*, 180, 92
- Quarles, B., Eberle, J., Musielak, Z. E., & Cuntz, M. 2011, *A&A*, 533, A2
- Rein, H. & Tamayo, D. 2016, *MNRAS*, 459, 2275
- Sartorello, S., Di Cintio, P., Trani, A. A., & Pasquato, M. 2025, *A&A*, 698, A28
- Shannon, C. E. & Weaver, W. 1949, *The mathematical theory of communication*
- Shatilov, D., Levichev, E., Simonov, E., & Zobov, M. 2011, *Physical Review Accelerators and Beams*, 14, 014001
- Shevchenko, I. I. & Mel'nikov, A. V. 2003, *Soviet Journal of Experimental and Theoretical Physics Letters*, 77, 642
- Shiozawa, K. & Tokuda, I. T. 2024, *Physics Letters A*, 510, 129531
- Sideris, I. V. & Kandrup, H. E. 2002, *Phys. Rev. E*, 65, 066203
- Sinai, Y. 1959, *Doklady Akademii Nauk SSSR*, 124, 768
- Skokos, C. 2001, *Journal of Physics A Mathematical General*, 34, 10029
- Skokos, C. 2010, in *Lecture Notes in Physics*, Berlin Springer Verlag, ed. J. Souchay & R. Dvorak, Vol. 790, 63–135
- Skokos, C., Bountis, T. C., & Antonopoulos, C. 2007, *Physica D Nonlinear Phenomena*, 231, 30
- Skokos, C. & Gerlach, E. 2010, *Phys. Rev. E*, 82, 036704
- Vallejo, J. C., Viana, R. L., & Sanjuán, M. A. F. 2008, *Phys. Rev. E*, 78, 066204
- Weiss, M., Hufnagel, L., & Ketzmerick, R. 2003, *Phys. Rev. E*, 67, 046209
- Wiesel, W. E. 1993, *Phys. Rev. E*, 47, 3686
- Yoshida, H. 1990, *Physics Letters A*, 150, 262
- Yoshida, H. 1993, *Celestial Mechanics and Dynamical Astronomy*, 56, 27